Nanometer-Scale Distribution of a Lubricant Modifier on Iron Films: A Frequency-Modulation Atomic Force Microscopy Study Combined with a Friction Test

Moriguchi, Shiho
Tsujimoto, Teppei
Sasahara, Akira
Kokawa, Ryohei
Onishi, Hiroshi

(Citation)
ACS Omega,4(17):17593-17599

(Issue Date)
2019-10-22

(Resource Type)
journal article

(Version)
Version of Record

(URL)
https://hdl.handle.net/20.500.14094/90006505

ACS OMEGA

Article

Cite This: ACS Omega 2019, 4, 17593−17599

http://pubs.acs.org/journal/acsodf

Nanometer-Scale Distribution of a Lubricant Modifier on Iron Films: A Frequency-Modulation Atomic Force Microscopy Study Combined with a Friction Test

Shiho Moriguchi,[†,‡] Teppei Tsujimoto,[§] Akira Sasahara,[†] Ryohei Kokawa,[∥] and Hiroshi Onishi*[,†]

[†]Department of Chemistry, School of Science, Kobe University, Rokko-dai, Nada-ku, Kobe 657-8501, Japan

[‡]Shimadzu Techno-Research Incorporated, Nishinokyo-shimoaicho, Nakagyo-ku, Kyoto 604-8436, Japan

[§]JXTG Nippon Oil & Energy Corporation, Chidoricho, Naka-ku, Yokohama 231-0815, Japan

[∥]Shimadzu Corporation, Nishinokyo-Kuwabaracho, Nakagyo-ku, Kyoto 604-8511, Japan

Supporting Information

ABSTRACT: Liquid lubricants used in mechanical applications are low-vapor-pressure hydrocarbons modified with a small quantity of polar compounds. The polar modifiers adsorbed on the surface of sliding solids dominate the friction properties when the sliding surfaces are in close proximity. However, a few methods are available for the characterization of the adsorbed modifiers of a nanometer-scale thickness. In this study, we applied frequency-modulation atomic force microscopy to evaluate the vertical and lateral density distributions of the adsorbed modifier in a real lubricant, namely, poly-α-olefin (PAO) modified with an orthophosphoric acid oleyl ester. The liquid-induced force on the probing tip was mapped on a plane that was perpendicular to the lubricant−iron interface with a force sensitivity on the order of 10 pN. The PAO in the absence of the ester modifier was directly exposed to the film, which produced a few liquid layers parallel to the film surface with layer-to-layer distances of 0.6−0.7 nm. A monomolecular layer of the modifier was intermittently adsorbed with increasing ester concentration in the bulk lubricant, with complete coverage seen at 20 ppm. The $C_{18}H_{35}$ chains of the oleyl esters fluctuating in the lubricant produced a repulsive force on the tip, which monotonically decayed with the tip-to-surface distance. The dynamic friction coefficient of sliding steel−lubricant−steel interfaces, which was separately determined using a friction tester, was compared with the force map determined on the iron film immersed in the corresponding lubricant. The complete monomolecular layer of the ester modifier on the static lubricant−iron boundary is a requirement for achieving smooth and stable friction at the sliding interface.

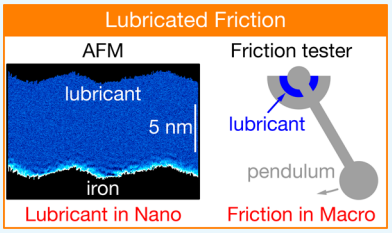

INTRODUCTION

Most liquid lubricants used in mechanical applications are low-vapor-pressure hydrocarbons modified with a small quantity of polar compounds. The polar modifiers are adsorbed on the surface of sliding solids, typically steel objects. When the sliding surfaces are close, the adsorbed monomolecular[1] or multimolecular[2] layers of the modifiers dominate the contact across the sliding interface, the sliding boundary in tribological terminology. In these circumstances, which are recognized as boundary lubrication, the adsorbed layers and hydrocarbon liquid covering the layers form an easily sheared film to minimize adhesion and wear.[3] Boundary lubrication may also involve mechanochemical reactions on the sliding interface. Reaction products, if any, provide layers with low shear strength covering the solid, i.e., tribolayers. The viscosity of the bulk lubricant plays a limited role in boundary lubrication. Controlling the lubricants at the boundary is the key to smooth sliding and stable friction.

The conception of boundary lubrication has been proposed and accepted since 1920. On the other hand, even today, it is not easy to characterize adsorbed modifiers of a nanometer-scale thickness. They are always buried in lubricant−solid interfaces. Electron-based methods for surface analysis do not function there. In situ, hopefully, operando methods working in lubricants should be developed since weakly adsorbed modifiers leave the surface when the surrounding lubricant is removed. The mass of adsorbed modifiers was determined with microbalance sensors.[4,5] Infrared absorption,[6−8] Raman scattering,[9] and sum-frequency generation[10] provided vibrational spectra of adsorbed modifiers to estimate their chemical structure. The layer thickness of deuterium-labeled modifiers was evaluated in a sub-nanometer precision by fitting neutron reflectivity as a function of scattering vector length.[11,12] Recently, Hirayama et al.[13] applied frequency-modulation atomic force microscopy (FM-AFM) for visualizing palmitic acid modifier layers on copper films immersed in a hexadecane-based model lubricant. The layers were so soft that they required a 10 pN-order force sensitivity for detecting the layer-induced force response.

In the present study, a representative hydrocarbon lubricant in commerce, poly-α-olefin, is modified with different quantities of a phosphoric acid alkyl ester, one of the

Received: September 1, 2019
Accepted: September 24, 2019
Published: October 7, 2019

frequently used modifiers in real lubricants.[14] The presence or absence of modifier layers is probed on iron films using FM-AFM. The vertical as well as lateral distribution of the layers is visualized by mapping layer-induced force on the probing tip. Furthermore, the dynamic friction coefficient of steel−lubricant−steel interfaces is separately determined with a friction tester. The macroscopic friction property as a function of modifier quantity is compared with the nanometer-scale distribution of the modifier layers.

MATERIALS

Lubricants. Nonpolar poly-α-olefin (PAO) was modified with orthophosphoric acid oleyl ester (C18AP). The chemical structure of the two compounds is illustrated in Figure 1. PAO

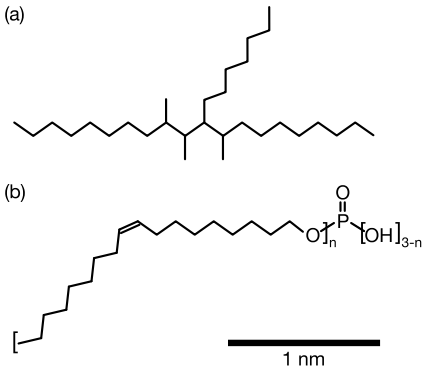

Figure 1. Lubricants. (a) Decene trimer as the major component in the poly-α-olefin (PAO) used in this study. The longest (C_{20}) alkyl chain is depicted in the all-*trans* conformation. (b) Orthophosphoric acid oleyl ester with n = 1 or 2 (C18AP).

(Ineos, Durasyn164) containing decene trimers ($C_{30}H_{62}$) as the major component was purified with activated clay. The purified liquid possessed a dynamic viscosity of 4 mm^2 s^{-1} at 100 °C. C18AP (Johoku Chemicals, JP-518) was a 1:1 mixture of the monoester and diester of the phosphoric acid. The modifier concentrations were adjusted at 0.2, 2, 20, and 200 ppm to simulate that in real lubricants, ca. 200 ppm.

Iron Films. Metallic iron was sputtered on silicon wafers to produce 50 nm-thick films. The films were naturally oxidized in air at room temperature (RT). Highly oriented pyrolytic graphite was compared with the iron films as a benchmark of solid with little chemical affinity to the phosphoric acid ester.

RESULTS AND DISCUSSION

AFM Method. Frequency-modulation detection of force on the probing tip was carried out with an SPM-8100FM microscope (Shimadzu). In topographic imaging of iron films, the resonance oscillation of a silicon cantilever (Nanoworld, PPP-NCHAuD) was mechanically excited with a piezoactuator. The nominal spring constant of the cantilevers was 42 N m^{-1}. The oscillation amplitude was regulated at a preset amplitude (A). When a lubricant-induced conservative force was loaded on the tip, the resonance frequency of cantilever oscillation (f) shifted accordingly. The topography of the scanned film was traced with regulation of the tip−surface distance by keeping the frequency shift (Δf) at a prefixed setpoint. The resonant frequency of the cantilevers was 100−140 kHz, and the quality factor of oscillation resonance was 2−3 in the lubricants. The typical spectrum of thermally induced cantilever oscillation is shown in Figure 2.

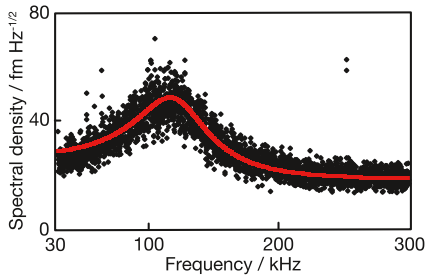

Figure 2. Typical spectrum of cantilever oscillation in PAO. Observed spectral density is presented with dots. A Lorentzian function (red line) fitted the observed data with a quality factor of 2 and a background spectral density of 18 fm Hz$^{-1/2}$.

An iron film or graphite wafer was fixed in a quartz Petri dish placed on the microscope stage driven by a piezoelectric scanner. The dish was filled with 500 μL of lubricant and then the cantilever assembly was put on top. Imaging scans were conducted at RT.

Iron Film Topography. Figure 3 presents the topographic images of the iron films observed in (a) pure PAO and (b)

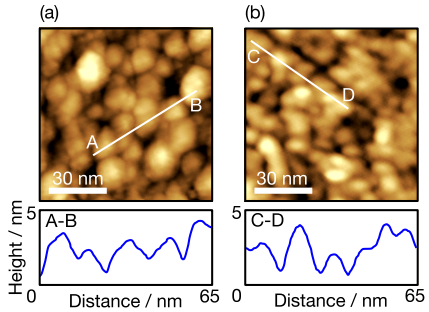

Figure 3. Topography of the iron films observed in the lubricants. The concentrations of C18AP were (a) 0 ppm and (b) 200 ppm. Image size, 90 nm^2; peak-to-peak amplitude of cantilever oscillation, 2.0 nm; and frequency shift setpoint, +83 Hz. The cross sections determined along the A−B and C−D lines are shown in the corresponding lower panels.

PAO containing 200 ppm C18AP, which was the highest concentration evaluated in this study. The spherical grains were recognized in the images. The lateral and vertical dimensions of the grains were between 5 and 20 nm and between 1 and 3 nm, respectively. The grain sizes were identical in both the films. However, the grain topography was sharper in image (a) as compared with image (b) in Figure 3. The reduced sharpness in image (b) could not be attributed to the different shapes of the probing tip, although different cantilevers were used for acquiring the two topographic images. A second set of images that were obtained in the presence and absence of C18AP is shown in Figure S1 in the Supporting Information. The grains in the C18AP-containing lubricant again exhibited features with reduced sharpness. The reproducible results suggest that the iron films were most likely covered by a soft material such as adsorbed C18AP, which resulted in the grain topography being less sharper than that of the uncovered films.

Force Mapping. The difference in the topographic sharpness seen in Figure 3 suggests that the C18AP layers were deposited on the iron films. In the presence of C18AP on the films, the phosphoric acid end should be in contact with

DOI: 10.1021/acsomega.9b02821
ACS Omega 2019, 4, 17593−17599

the naturally oxidized iron films, with an expansion of the $C_{18}H_{35}$ chains into the lubricant liquid. In this subsection, the mechanical response of the expanding chains is probed and mapped on the planes that are perpendicular to the iron films to verify C18AP deposition.

Figure 4 shows the Δf maps that were observed in the lubricants containing different concentrations of C18AP. The

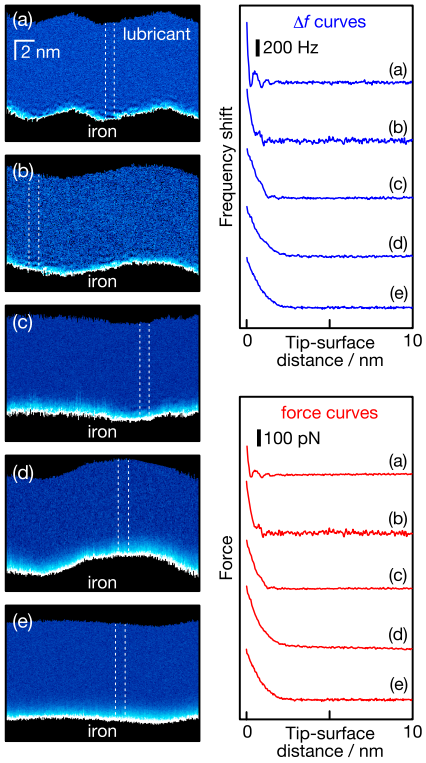

Figure 4. Lubricants over the iron films. The cross-sectional Δf distribution was mapped on a plane that was perpendicular to the film surface in the lubricants containing C18AP at (a) 0 ppm, (b) 0.2 ppm, (c) 2 ppm, (d) 20 ppm, and (e) 200 ppm. The amplitude of the cantilever oscillation was 0.4 nm. The aspect ratio of the lateral and vertical scales has been tuned unity in the maps. A large (or small) positive Δf is depicted using a bright (or dark) blue color. Fourteen Δf–distance curves situated between the two dashed lines were averaged, with the results shown in the upper right panel. The averaged Δf–distance curves were converted to force–distance curves as depicted in the lower right panel.

oscillating cantilever was scanned vertically from the bulk lubricant to the iron film. The frequency shift as a function of the vertical coordinate was simultaneously recorded to obtain one Δf–distance curve composed of 250 pixels at one lateral position. We aborted the vertical scan when Δf reached a predetermined threshold (+600 Hz for the acquired maps in Figure 4); the cantilever was retracted into the lubricant by 10 nm to prevent extensive tip-to-surface contact. We repeatedly acquired 256 or 512 vertical scans along a 20 nm-long lateral coordinate. One Δf map was subsequently constructed on a plane perpendicular to the iron film with an acquisition time of 26 (51) s for 256 (512) scans per frame.

The observed Δf map can be considered to be an approximate distribution of the lubricant-induced repulsive force on the tip. A repulsive force causes a positive Δf, although the relation between the force and Δf is nonlinear.[15] A large (small) value of Δf is denoted by a bright (dark) blue color in Figure 4, while areas outside the scanned range are shown in black. The brightest region at the base of each map represents the boundary between the lubricant liquid and iron film. The repulsive force on the tip increased monotonically when it was moved deeper into this region, signifying tip-to-surface contact. The envelope of the brightest region was corrugated to trace the topography of the iron films. The lateral and vertical dimensions of the corrugation were typically 10 and 1–2 nm, respectively. The corrugations along these dimensions were consistent with the topographic images shown in Figure 3.

The frequency shift, i.e., the force on the tip, was uneven in the vicinity of the iron film. Fourteen Δf–distance curves were obtained between the two dashed lines and averaged, as shown in the upper right panel of Figure 4. The zero tip-to-surface distance in the Δf–distance curve was defined at the vertical coordinate of the tip where Δf exceeded the threshold, +600 Hz. The averaged Δf–distance curve was then converted to a force–distance curve using the Sader–Jarvis formula[15] and is shown in the lower right panel of Figure 4. The signal-to-noise ratio in the converted curve showed a force sensitivity on the order of 10 pN in the PAO.

It was technically not easy to average the whole set of Δf curves in the map. The iron film surface, where the tip-to-surface distance was defined to be zero, was not flat. The vertical scans were aborted in force mapping when Δf exceeded the preset threshold. However, the force on the tip was not constant at the aborted positions since the force is given by a weighed integration of Δf along the tip trajectory as formulated by Sader and Jarvis.[15] We recognized by visual inspection that the features in the map were almost homogeneous along the lateral coordinate even on the corrugated film surface. On this recognition, averaging a limited number of Δf curves, 14 curves in Figure 4, provided a reasonable way to improve the statistical reliability of representative curve on the examined interface.

Alternating dark and bright layers appeared in the map (Figure 4a) when we used pure PAO, suggesting that the film was covered by two or three PAO liquid layers. The distance between the neighboring maxima in the corresponding force curve was in the range of 0.6–0.7 nm. The liquid PAO layers were suggested to be separated by this distance over the iron film. The liquid-induced force pushing or pulling the tip apex is attributed to the local liquid density, although the force–density relation is not straightforward. In a solvent-tip approximation developed for an ideal tip as small as liquid molecules,[16,17] the liquid molecules surrounding the apex generate the force in the form of local free-energy gradient. With a macroscopic force probe, which has been used in surface force apparatus, the force on the probe is simply proportional to the local density of liquid molecules.

Liquid layers separated by 0.6–0.7 nm have been found in the force maps of organic liquids and assigned to the linear hydrocarbon chains that lie flat over the solid surface. *n*-Dodecane and *n*-hexadecane liquid in contact to a CH_3-terminated thiolate monolayer resulted in liquid layers separated by 0.56–0.58 nm.[18] *n*-Hexadecane exhibited layer-to-layer distances of 0.6 and 0.4–0.6 nm on Cu films[13] and graphite wafers,[19,20] respectively. Oxygenated chains such as *n*-decanol,[21,22] *n*-dodecanol,[23] and tetraglyme ($CH_3(OCH_2CH_2)_4OCH_3$)[24] produced liquid layers separated by 0.5–0.6 nm on graphite. The carbon chain branching of the PAO used in this study is illustrated in Figure 1. The branched

DOI: 10.1021/acsomega.9b02821
ACS Omega 2019, 4, 17593–17599

chain showed a layer-to-layer distance (0.6−0.7 nm) that was slightly larger than that observed in the linear-chain compounds mentioned above (0.4−0.6 nm). This result is not surprising as a heavily branched hydrocarbon such as 2,6,10,15,19,23-hexamethyltetracosane (squalane) has previously produced liquid layers separated by 0.6 nm on graphite.[25] A recent AFM study[26] reported averaged layer distances of 0.42 and 0.47 nm in a larger PAO, decene tetramers, on graphite and steal, respectively.

The layered force distribution weakened and in cases even disappeared when C18AP was added to PAO. The PAO layers intermittently remained in the map (Figure 4b) at a C18AP concentration of 0.2 ppm, while the layered feature almost disappeared in the map (Figure 4c) at a concentration of 2 ppm. The repulsive force on the tip monotonically decayed with the increase in tip-to-surface distance in the areas where the layered feature disappeared. Here, the laterally heterogeneous layers of the lubricant modifier were visualized on a nanometer-scale resolution in space. The layered structure was completely removed by adding C18AP at concentrations of 20 and 200 ppm, as shown in the maps in Figure 4d,e.

The monotonically decaying force component increased with an increase in C18AP concentration. The decay length, which was defined as the tip-to-surface distance resulting in zero force, was estimated to be 0.6, 0.9, and 2.0 nm, corresponding to C18AP concentrations of 0.2, 2, and 20 ppm, respectively. A further increase in the concentration to 200 pm caused little extension in the decay length. This resulted in the two force curves at 20 and 200 ppm being identical. The identical force curves were a reflection of the C18AP layer that fully covered the iron films. Here, we assume that the acid esters were anchored at the phosphoric acid end on the naturally oxidized iron films. Each adsorbed C18AP contains one or two $C_{18}H_{35}$ chains that extend into the lubricant liquid. The chains could not be as closely packed like the alkyl chains of alkylthiolates on a gold film because the C18AP used in this study was a mixture of the monoester and diester. The loosely packed chains have to be flexible and fluctuating in the lubricant. The force on the tip was fluctuating when it was in contact with a fluctuating chain. The accumulation time at each vertical coordinate was typically 30 μs in our force mapping scans. Hence, the observed Δf represented the time-averaged force on the tip and in turn reflected the time-averaged density distribution of the fluctuating chains. The observed curves decayed to zero force at a tip-to-surface distance of 2.0 nm at high C18AP concentrations. This distance is consistent with the $C_{18}H_{35}$ chain length depicted in Figure 1, wherein the two terminal carbon atoms are separated by 1.9 nm. The observed length saturated at 2.0 nm, which suggests that there was a monomolecular C18AP layer on the iron films. The undersaturated layers generated at 0.2 and 2 ppm exhibited short decay lengths. The $C_{18}H_{35}$ chains in the unsaturated layers can be tilted to enable contact with the film to gain van der Waals energy. The tilted chains presented thin layers.

The alkyl chains in the alkylthiolate monolayers prepared on a gold film were closely packed to solidify the monolayers. The solidified monolayer created a static boundary with the organic solvents that could be traced during topographic imaging with FM-AFM.[18] We assume that the C18AP layers on the iron films were not solidified. Force mapping facilitated the quantification of the vertical and lateral distributions of the C18AP layers having a fluctuating, dynamic boundary with the liquid PAO. Fukuma and co-workers demonstrated the feasibility of AFM-based force mapping for estimating the time-averaged density distribution of the lipid head groups[27] and biofouling-resistant moieties[28] in water. Hirayama et al.[13] extended their method to include a hexadecane-based model lubricant that is more viscous than water. Moustafa et al.[29] conducted a bimodal AFM study to visualize the lateral distribution of weakly adsorbed organic aggregates over graphite surfaces. A recent mapping study on a liquid ester lubricant with no modifier[30] reported the deposition of soft layers on a diamondlike carbon film following rubbing in a friction test, which was most likely a result of the tribochemical reactions of the lubricant. Our present study provided the lateral and vertical distributions of the ester modifiers in the poly-α-olefin liquid. The relation between the observed distribution of the modifier and the macroscopic friction property is examined in the final section of this paper.

Force mapping in the lubricants was further examined using graphite wafers to support the interpretation of the C18AP layer deposition on the iron films. Graphite was considered to have little chemical affinity to the phosphoric acid ester. Figure 5 shows the Δf maps that were observed in the absence and

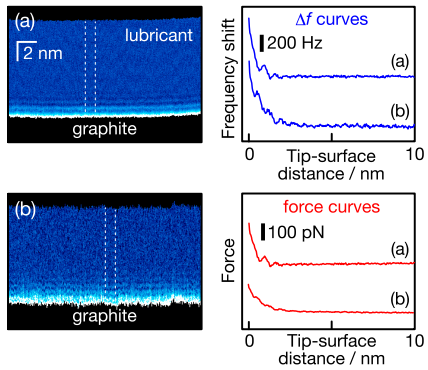

Figure 5. Lubricants over graphite. The Δf maps were obtained for the lubricants with C18AP concentrations of (a) 0 ppm and (b) 200 ppm. Fourteen Δf−distance curves situated between the two dashed lines were averaged, with the results shown in the upper right panel. The averaged Δf−distance curves were converted to force−distance curves, as depicted in the lower right panel. The cantilever oscillation amplitude: (a) 0.6 nm and (b) 0.4 nm.

presence of C18AP. The freshly cleaved graphite wafer showed atomically flat terraces in the topographic images (not shown). The map (Figure 5a) captured in pure PAO shows that the envelope of the brightest colored region, which represents the physical topography of the wafer, was straight as expected. Three liquid layers appeared with layer-to-layer distances of 0.6−0.7 nm. The layered PAO liquid was seen both on the graphite and iron films. Figure 5b shows the Δf map acquired in the presence of C18AP at 200 ppm. Three bright layers parallel to the graphite surface were still identifiable, indicating that the lubricant liquid was directly exposed to the graphite. The force mapping results shown in Figures 4 and 5 support our interpretation that the iron film was partially or fully covered by the C18AP layers depending on the concentration of C18AP in the bulk lubricant.

In addition to the layered feature, a monotonically decaying force was to a limited extent identified in the C18AP-containing lubricant. The decay length was estimated to be ca. 2 nm, although overlapped with the oscillatory force. A limited

DOI: 10.1021/acsomega.9b02821
ACS Omega 2019, 4, 17593−17599

amount of C18AP might have been adsorbed on the graphite surface and/or the probing tip apex to produce the monotonically decaying force overlapping the oscillatory force coming from PAO layers. Comparing ordinary silicon tips with tips coated or made of carbonaceous materials would help us to interpret the monotonically decaying force recognized on graphite.

Friction Test Method. The dynamic friction coefficient at the sliding steel−lubricant−steel interfaces was evaluated using a pendulum-type friction tester (Narita Seiki Inc.).[31] A steel pendulum was freely oscillated with the fulcrum dipped in the lubricant (see the table of contents graphic). One oscillation was typically completed in 4 s. The amplitude of the pendulum oscillation was dampened because of the lubricated friction on the fulcrum. The initial amplitude (A_0) was set at 0.5 rad, and the decayed amplitude (A_k) was recorded on the basis of the number of completed oscillations (k) until $A_k \leq 0.1$. The friction coefficient (μ), which was averaged over one measurement ranging from A_0 to A_n, can be expressed by the following equation

$$\mu = C \times \frac{\sum_{k=1}^{n} (A_0 - A_k)}{\sum_{k=1}^{n} k}$$

where n is the number of recorded oscillations in each measurement run. Using our tester, we calibrated the constant C to 3.2 according to the pendulum length and weight of the fulcrum. The friction coefficient increased with repeated oscillation cycles. Hence, a maximum of 20 measurement runs were conducted to trace the time course of the coefficient.

Friction Coefficient at Different Modifier Concentrations. Figure 6 shows the evaluated coefficients in the lubricants containing C18AP concentrations of 0, 2, 20, and 200 ppm. The raw amplitudes (A_k) recorded in the individual runs are reported in the Supporting Information. The coefficient for pure PAO was 0.11 in run 1, rapidly increased to 0.34 in runs 4−13, and continued to increase up to 0.40 in runs 14−20. The friction increased with the sliding cycles in the modifier-free PAO, which resulted in the adhesion of the sliding steel surfaces. The coefficient for a C18AP concentration of 2 ppm similarly increased in runs 1−13 and subsequently remained constant between 0.33 and 0.34 in runs 14−20. The limited amount of C18AP caused a noticeable change in the friction at the sliding interface. The friction further decreased when the C18AP concentration was increased to 20 ppm. The initial coefficient (0.12) was constant until run 5, increased in runs 6−17, and remained almost constant between 0.26 and 0.28 in runs 18−20. The addition of C18AP at 200 ppm, which was the highest concentration investigated, stabilized the coefficient between 0.11 and 0.10 in runs 1−10. The stable, low friction that was observed at this concentration is a characteristic of the lubricants that have been successfully modified with polar compounds.

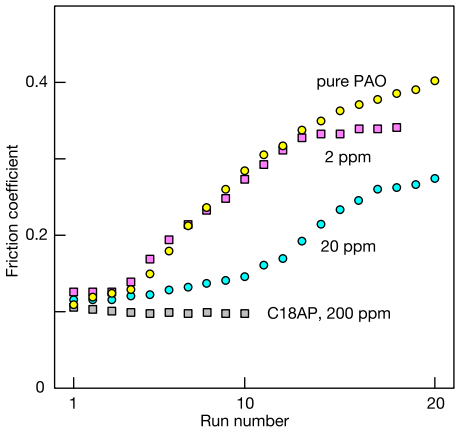

Figure 6. Friction coefficient of the steel−lubricant−steel interfaces that were evaluated using a pendulum-type friction tester. Lubricants containing C18AP concentrations of 0, 2, 20, and 200 ppm were tested.

Compare the friction results with the nanometer-scale force mapping results described in the previous section. In the absence of the modifier, layered PAO liquid was present on the iron film. The steal surfaces sliding in the fulcrum should also have been exposed to PAO and hence adhered. The time course of the friction coefficient was modified partially at a lower concentration (2 ppm), at which concentration the layered PAO feature almost disappeared in the force map on the film. The force map at 20 ppm showed a full coverage of the C18AP monolayer on the film. The macroscopic friction continued to decrease in the lubricant with this modifier concentration. The force map was insensitive to further addition of C18AP, while the friction coefficient still descended at 200 ppm.

We infer that the friction and force map results are qualitatively related, even though one was observed at the sliding steel−lubricant−steel interface and the other at the static lubricant−iron boundary. A C18AP monolayer that completely covers the surface of a solid in a static environment is a requirement for the modification of the friction property in the sliding condition. The excess modifier in the bulk lubricant may have additionally contribute to produce phosphorus-containing tribolayers on the sliding fulcrum interface, leading to the stable low friction achieved at 200 pm.

Our approach that proposes force mapping with FM-AFM provides a unique opportunity for characterizing modifier-containing lubricants. The presence of PAO-induced layers indicates that the solid surface under investigation was directly exposed to the lubricant. The surface was covered with flexible moieties of the modifier fluctuating in the lubricant liquid when the force on the probing tip monotonically decayed as a function of the tip-to-surface distance. The vertical distribution of the monotonically decaying force was a reflection of the thickness of the modifier layer deposited on the surface. The dynamic friction coefficient at the real sliding interfaces having macroscopic dimensions responded to the nanometer-scale distribution of the modifier layer when mechanically probed by the AFM tip.

One potential advantage of the AFM-based method for modifier characterization is the nanometer-scale resolution of the lateral coordinates over the solid surface. The other methods mentioned in the Introduction section provide the mass, chemical structure, or layer thickness of the deposited modifier averaged over a millimeter-sized lubricant−solid interface. Real modifier layers can be heterogeneous, particularly in the presence of two or more modifiers. Rubbing the layers may induce further heterogeneity. AFM-based force mapping is a standalone technique for locally characterizing the lubricant modifiers in the buried interfaces.

DOI: 10.1021/acsomega.9b02821
ACS Omega 2019, 4, 17593−17599

CONCLUSIONS

We demonstrated the feasibility of using FM-AFM for mechanically probing a lubricant−solid interface, C18AP-containing PAO covering the iron films. We mapped the lubricant-induced force on the probing tip two-dimensionally on a plane that was perpendicular to the lubricant−iron interface and thus achieved a force sensitivity and spatial resolution on the order of 10 pN and 10 pm, respectively. We propose the following conclusions after interpretation of the observed force maps. The PAO was directly exposed to the naturally oxidized iron film in the absence of the C18AP modifier, and it exhibited a few liquid layers parallel to the film surface with a layer-to-layer distance of 0.6−0.7 nm. C18AP, if any in the lubricant, was adsorbed with its phosphoric acid end anchored to the films. There was fluctuation of the $C_{18}H_{35}$ chains of C18AP in the lubricant. The force maps reflected the time-averaged density distribution of the fluctuating chains, which monotonically decayed to zero force at a tip-to-surface distance of 2 nm when a monomolecular layer of C18AP was completed. The PAO liquid layers were intermittently removed in the lubricants containing C18AP concentrations of 0.2 and 2 ppm; they completely disappeared at 20 and 200 ppm. The iron film that was completely covered with the C18AP layer produced topographic images with reduced sharpness according to its fluctuating, dynamic boundary with the lubricant. The dynamic friction coefficient of the sliding steel−lubricant−steel interfaces, which was separately determined using the friction tester, decreased with increasing the coverage of the monomolecular C18AP on the iron film. The mechanical probing with FM-AFM combined with friction test offers a promising technique for bridging nanometer-scale lubricant distribution and sliding friction in the macroscopic dimensions.

ASSOCIATED CONTENT

Supporting Information

The Supporting Information is available free of charge on the ACS Publications website at DOI: 10.1021/acsomega.9b02821.

Iron film topography; friction test raw results; pendulum amplitudes in PAO (PDF)

AUTHOR INFORMATION

Corresponding Author

*E-mail: oni@kobe-u.ac.jp.

ORCID

Hiroshi Onishi: 0000-0003-1873-9105

Author Contributions

The manuscript was written through contributions of all authors.

Notes

The authors declare no competing financial interest.

ACKNOWLEDGMENTS

Tomoko Hirayama in Doshisha University provided the iron films. This study was partially supported by JSPS KAKENHI grant number JP18K19058.

REFERENCES

(1) Hardy, W. B.; Doubleday, I. Boundary Lubrication−The Paraffin Series. *Proc. R. Soc. London, Ser. A* **1922**, *100*, 550−574.

(2) Allen, C. M.; Drauglis, E. Boundary Layer Lubrication: Monolayer or Multilayer. *Wear* **1969**, *14*, 363−384.

(3) Zhang, C. Understanding the Wear and Tribological Properties of Ceramic Matrix Composites. In *Advances in Ceramic Matrix Composites*; Low, I. M., Ed.; Woodhead Publishing, 2014; pp 312−339.

(4) Müller, M. T.; Yan, X.; Lee, S.; Perry, S. S.; Spencer, N. D. Lubrication Properties of a Brushlike Copolymer as a Function of the Amount of Solvent Absorbed within the Brush. *Macromolecules* **2005**, *38*, 5706−5713.

(5) Evans, K. O.; Biresaw, G. Quartz crystal microbalance investigation of the structure of adsorbed soybean oil and methyl oleate onto steel surface. *Thin Solid Films* **2010**, *519*, 900−905.

(6) Cann, P. M.; Spikes, H. A. In-Contact IR Spectroscopy of Hydrocarbon Lubricants. *Tribol. Lett.* **2005**, *19*, 289−297.

(7) Mangolini, F.; Rossi, A.; Spencer, N. D. Chemical Reactivity of Triphenyl Phosphorothionate (TPPT) with Iron: An ATR/FT-IR and XPS Investigation. *J. Phys. Chem. C* **2011**, *115*, 1339−1354.

(8) Sasaki, K.; Inayoshi, N.; Tashiro, K. Development of new in situ observation system for dynamic study of lubricant molecules on metal friction surfaces by two-dimensional fast-imaging Fourier-transform infrared-attenuated total reflection spectrometer. *Rev. Sci. Instrum.* **2008**, *79*, No. 123702.

(9) Bongaerts, J. H. H.; Day, J. P. R.; Marriott, C.; Pudney, P. D. A.; Williamson, A.-M. *In situ* confocal Raman spectroscopy of lubricants in a soft elastohydrodynamic tribological contact. *Appl. Phys. Lett.* **2008**, *104*, No. 014913.

(10) Watanabe, S.; Nakano, M.; Miyake, K.; Sasaki, S. Analysis of the Interfacial Molecular Behavior of a Lubrication Film of *n*-Dodecane Containing Stearic Acid under Lubricating Conditions by Sum Frequency Generation Spectroscopy. *Langmuir* **2016**, *32*, 13649−13656.

(11) Hirayama, T.; Torii, T.; Konishi, Y.; Maeda, M.; Matsuoka, T.; Inoue, K.; Hino, M.; Yamazaki, D.; Takeda, M. Thickness and density of adsorbed additive layer on metal surface in lubricant by neutron reflectometry. *Tribol. Int.* **2012**, *54*, 100−105.

(12) Wood, M. H.; Casford, M. T.; Steitz, R.; Zarbakhsh, A.; Welbourn, R. J. L.; Clarke, S. M. Comparative Adsorption of Saturated and Unsaturated Fatty Acids at the Iron Oxide/Oil Interface. *Langmuir* **2016**, *32*, 534−540.

(13) Hirayama, T.; Kawamura, R.; Fujino, K.; Matsuoka, T.; Komiya, H.; Onishi, H. Cross-Sectional Imaging of Boundary Lubrication Layer Formed by Fatty Acid by Means of Frequency-Modulation Atomic Force Microscopy. *Langmuir* **2017**, *33*, 10492−10500.

(14) *Lubricant Additive, Chemistry and Applications*, 2nd ed.; Rudnick, L. R., Ed.; Culinary and Hospitality Industry Publications Services, 2009.

(15) Sader, J. E.; Jarvis, S. P. Accurate formulas for interaction force and energy in frequency modulation force spectroscopy. *Appl. Phys. Lett.* **2004**, *84*, 1801−1803.

(16) Reischl, B.; Watkins, M.; Foster, A. Free Energy Approaches for Modeling Atomic Force Microscopy in Liquids. *J. Chem. Theory Comput.* **2013**, *9*, 600−608.

(17) Amano, K.; Suzuki, K.; Fukuma, T.; Takahashi, O.; Onishi, H. The Relationship between Local Liquid Density and Force Applied on A Tip of Atomic Force Microscope: A Theoretical Analysis for Simple Liquids. *J. Chem. Phys.* **2013**, *139*, No. 224710.

(18) Hiasa, T.; Kimura, K.; Onishi, H. Two-Dimensional Distribution of Liquid Hydrocarbons Facing Alkanethiol Monolayers Visualized by Frequency Modulation Atomic Force Microscopy. *Colloids Surf., A* **2012**, *396*, 203−207.

(19) Gosvami, N. N.; Sinha, S. K.; Hofbauer, W.; O'Shea, S. J. Solvation and squeeze out of hexadecane on graphite. *J. Chem. Phys.* **2007**, *126*, No. 214708.

(20) Van, L. P.; Kyrylyuk, V.; Polesel-Maris, J.; Thoyer, F.; Lubin, C.; Cousty, J. Experimental three-dimensional description of the liquid hexadecane/graphite interface. *Langmuir* **2009**, *25*, 639−642.

DOI: 10.1021/acsomega.9b02821
ACS Omega 2019, 4, 17593−17599

(21) Hiasa, T.; Kimura, K.; Onishi, H. Cross-Sectional Structure of Liquid 1-Decanol over Graphite. *J. Phys. Chem. C* **2012**, *116*, 26475−26479.
(22) de Beer, S.; Wennink, P.; van der Weide-Grevelink, M.; Mugele, F. Do epitaxy and temperature affect oscillatory solvation forces? *Langmuir* **2010**, *26*, 13245−13250.
(23) Hofbauer, W.; Ho, R. J.; Hairulnizam, R.; Gosvami, N. N.; O'Shea, S. J. Crystalline structure and squeeze-out dissipation of liquid solvation layers observed by small-amplitude dynamic AFM. *Phys. Rev. B* **2009**, *80*, No. 134104.
(24) Minato, T.; Araki, Y.; Umeda, K.; Yamanaka, T.; Okazaki, K.; Onishi, H.; Abe, T.; Ogumi, Z. Interface Structure between Tetraglyme and Graphite. *J. Chem. Phys.* **2017**, *147*, No. 124701.
(25) Gosvami, N. N.; Sinha, S. K.; O'Shea, S. J. Squeeze-out of branched alkanes on graphite. *Phys. Rev. Lett.* **2008**, *100*, No. 076101.
(26) Krass, M.-D.; Krämer, G.; Dellwo, U.; Bennewitz, R. Molecular Layering in Nanometer-Confined Lubricants. *Tribol. Lett.* **2018**, *66*, No. 87.
(27) Asakawa, H.; Yoshioka, S.; Nishimura, K.; Fukuma, T. Spatial Distribution of Lipid Headgroups and Water Molecules at Membrane/Water Interfaces Visualized by Three-Dimensional Scanning Force Microscopy. *ACS Nano* **2012**, *6*, 9013−9020.
(28) Molino, P. J.; Yang, D.; Penna, M.; Miyazawa, K.; Knowles, B. R.; MacLaughlin, S.; Fukuma, T.; Yarovsky, I.; Higgins, M. J. Hydration Layer Structure of Biofpuling-Resistant Nanoparticles. *ACS Nano* **2018**, *12*, 11610−11624.
(29) Moustafa, A. M. A.; Huang, J.; McPhedran, K. N.; Zeng, H.; El-Din, M. G. Probing the Adsorption of Weak Acids on Graphite Using Amplitude Modulation−Frequency Modulation Atomic Force Microscopy. *Langmuir* **2015**, *31*, 3069−3075.
(30) Okubo, H.; Sasaki, S. Frequency-Modulation Atomic Force Microscopic Observation for Ultralow Frictional Solid−Liquid Interface of Diamond−Like Carbon in an Environmentally Friendly Oil. *Tribol. Lett.* **2019**, *67*, No. 3.
(31) Noriyuki Soda (1911−1995), a mechanical engineer in Japan, originally designed the tester that the authors used in this study.

DOI: 10.1021/acsomega.9b02821
ACS Omega 2019, 4, 17593−17599